Published in IET Power Electronics
Received on 8th May 2012
Revised on 7th December 2012
Accepted on 23rd December 2012
doi: 10.1049/iet-pel.2012.0256

ISSN 1755-4535

Fault diagnosis scheme for open-circuit faults in field-oriented control induction motor drives

Diego Rivelino Espinoza-Trejo[1], Daniel Ulises Campos-Delgado[2], Guillermo Bossio[3], Ernesto Bárcenas[1], José Enrique Hernández-Díez[1], Luis Felipe Lugo-Cordero[1]

[1]*Coord. Acad. Región Altiplano, Univ. Aut. de San Luis Potosí, Matehuala, S.L.P., México*
[2]*Facultad de Ciencias, Univ. Aut. de San Luis Potosí, San Luis Potosí, México*
[3]*Grupo de Electrónica Aplicada, Univ. Nacional de Río Cuarto, Córdoba, Argentina*
E-mail: drespinozat@ieee.org

Abstract: In this study, a new model-based fault detection and isolation (FDI) strategy is proposed for field-oriented control (FOC) induction motor (IM) drives. Actuator faults are addressed, and specifically, single open-circuit faults are considered in this study. The residual signals are synthesised by taking the resulting closed-loop dynamics when a FOC strategy is applied, that is, the residuals are referenced to the synchronous reference frame (dq^e-coordinates), which are generated by using a bank of variable structure observers to obtain a robust FDI scheme. Thus, subsystems sensitive to a specific fault, but decoupled from other faults are obtained in a natural way, where only two stator currents and the mechanical position are required for fault isolation purposes. Residual evaluation is carried out in the stator reference frame (dq-coordinates) for the IM model, where the residual direction (angle) is employed to isolate a fault in each one of the six power switches in a voltage source inverter. In addition, the observer FDI scheme can be combined with a fault re-configuration strategy in order to improve the reliability of the motor drive. Experimental results are illustrated for a three-phase 3/4 HP IM drive at different reference frequencies and load torques with single open-circuit faults that verify the ideas presented in this work.

1 Introduction

Reliability is an important factor in modern variable speed drives, specially if the automated process is handling critical loads which could not tolerate a sudden stoppage. Factors such as transients, heavy loads and environmental conditions are the main stresses on this kind of systems. In [1], it is mentioned that around 38% of the faults in variable speed ac drives are because of failures in the power devices. In addition, according to Yang *et al.* [2], the semi-conductor devices are the most fragile components in power electronic converters. Hence, power electronics reliability is an important issue, and clearly an area with an active research community, see for example [2–4]. In this context, a novel model-based fault detection and isolation (FDI) scheme for power converter faults in voltage source inverters (VSI), feeding induction motors (IM) is proposed in this paper (see Fig. 1). Inverter power switch faults are divided into open-circuit F_1 and short-circuit F_2. In this study, only single open-circuit faults on the semi-conductor devices (IGBT's) in the VSI are considered, which are denoted by switches $sw_1 - sw_6$ in Fig. 1. In fact, this restriction does not limit the applicability of the proposed approach, since short-circuit faults trigger the over-current protections in the VSI (see Fig. 1), and as a consequence, the dynamic effect is equivalent to an open-circuit fault.

Some FDI methods for open-circuit faults have been previously suggested in literature [5–16]. For example, in [5] a fuzzy logic FDI system for open-circuit faults in PWM-VSI IM drives was proposed. The dq current trajectory is used in order to obtain the F_1 fault features. At the same time, fuzzy logic is suggested to isolate the six faults related to each switch in the VSI. In [6], once more the motor line currents in the stator reference frame are used (dq-coordinates). In this case, intermittent misfiring faults are diagnosed by using a pattern recognition philosophy. In both cases [5, 6], only an evaluation in open-loop V/Hz operation has been addressed. However, as was shown in [7], the dq current trajectory is seriously affected when the IM drive is operating under a closed-loop control action. In this way, most of the methods proposed previously in the literature, fail when they run under this condition. An alternative approach is to incorporate new measurements of the motor drive system, hence voltage sensors have been employed at certain key points of the VSI architecture in order to detect and isolate faults, as in [9, 10]. However, some of these techniques assume the availability of the neutral connection in the stator, which in some applications is not feasible. In addition, by including new hardware into the FDI scheme, the cost is increased and the reliability is reduced by these new components.

A survey paper of FDI techniques in power inverters can be found in [11]. In fact, the most recent works address two main

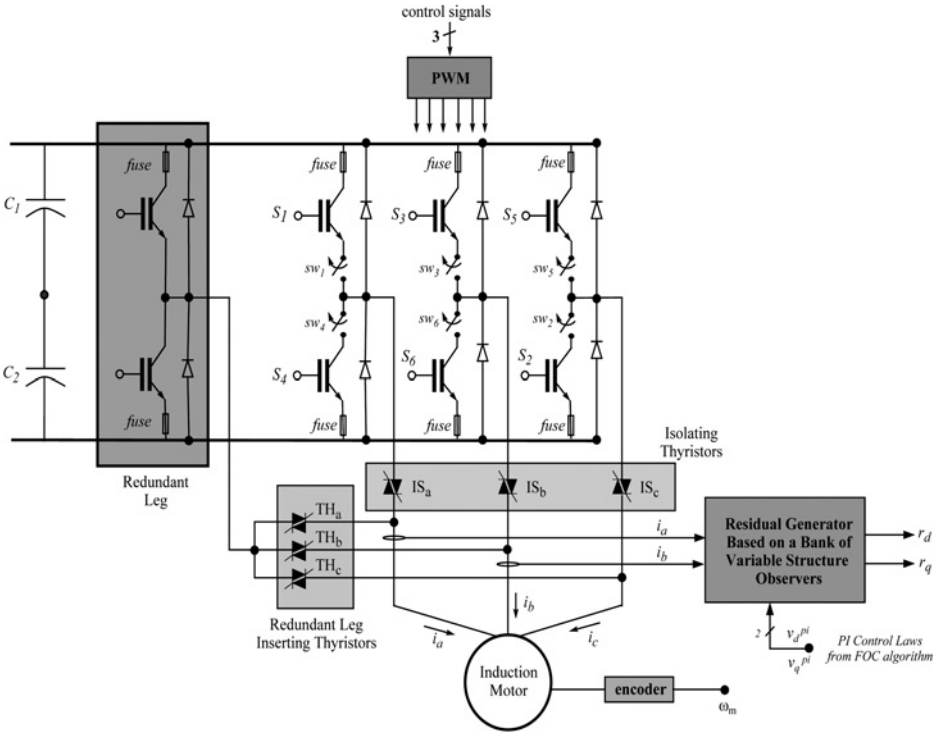

Fig. 1 *Configuration of the VSI post-fault operation [17]*

obstacles: (i) closed-loop operation [12–14] and (ii) concurrent faults [13, 15, 16]. For example in [12], a machine learning technique is presented, which requires both stator currents and voltages to detect and isolate open and short-circuit fault conditions under closed-loop field-oriented control FOC). In [13], a diagnostic algorithm for multiple open-circuit faults based on the reference current errors have been proposed for a vector controlled permanent magnet synchronous motor drive. Meanwhile in [14], a diagnostic method is suggested by using the switching function model, which minimises fault detection time and is available for open-loop and closed-loop control strategies. For concurrent faults in [15], an FDI algorithm based on non-linear observers has been proposed, which relies on the information of stator currents and mechanical velocity. Finally, Sleszynski *et al.* [16] describes an algorithm based on the *dq*-trajectory of the stator currents. In this case, a normalised dc-components method is evaluated for FDI purposes.

In this context, the proposed FDI scheme addresses one important open issue in the literature: open-circuits faults under closed-loop operation. At this stage, only single faults are addressed and simultaneous faults will be investigated in a subsequent study. The FOC algorithm is considered as case study, and the residual signals are synthesised by using the closed-loop FOC resulting dynamics. Note that, by considering the FOC strategy, two asymptotically decoupled and linear subsystems are obtained in closed-loop, which are the key information used for fault isolation [18, 19] and employed to obtain a robust FDI scheme insensible to load torque variations. Last, the main advantages of this FDI scheme are: (i) the FDI scheme is independent of the load torque and operating conditions (as for example low speed), (ii) the residual computation requires the information of two stator currents and mechanical positions, which are available under FOC closed-loop operation, (iii) the methodology has low-complexity and can be implemented in real-time and (iv) the FDI algorithm is capable of providing fast detection and isolation times in closed-loop operation. Concurrently, a possible disadvantage is the need of the IM parameters. However, this inconvenience can be compensated by introducing robustness to the residual generators through variable structure observers design.

Ultimately, the FDI scheme proposed in this work was briefly presented for the first time in [20], as a conference paper. However, only simulation results were considered in this first version. Now in this extended work, experimental results on a test bench of 3/4HP IM are reported in Section 5, a new residual definition is proposed (Section 3.1), as well as, an update of the state of the art in the field (Section 1). We also suggest a more recent fault reconfiguration strategy to the one presented in the previous version. Finally, with respect to FOC implementation, the rotor flux estimation was modified.

2 Induction motor modelling

In this section, the dynamic model of IMs is briefly reviewed. The reference frame suggested for FDI purposes is well-known as synchronous reference frame, and it is obtained by using a two-phase motor representation direct and quadrature axes ($d^e - q^e$ coordinates) [21], where dq^e axes are rotating to synchronism velocity ω_s. The IM physical parameters are stator and rotor self-inductances (L_s, L_r), mutual inductance L_m, stator and rotor equivalent resistances (R_s, R_r), moment of inertia J, mechanical friction f, number of pole pairs n_p and T_L denotes the load torque. Let $a = R_r / L_r$, $b = L_m / \sigma L_s L_r$, $c = \left(L_m^2 R_r / \sigma L_s L_r^2\right) + \left(R_s / \sigma L_s\right)$, $m = 3 n_p L_m / 2 J L_r$, $d = 1 / \sigma L_s$, $k = 1 / J$, $\sigma = 1 - \left(L_m^2 / L_s L_r\right)$ be a parametrisation of the IM model, where a, b, c, m, d, k and σ are known parameters and take $\left(v_d^e, v_q^e\right)^T$ as the input vector in the system. In this way, the

IET Power Electron., 2013, Vol. 6, Iss. 5, pp. 869–877
doi: 10.1049/iet-pel.2012.0256

resulting dynamic system showed in (1) is the mathematical model of the IM in the synchronous reference frame [21], which is formed by two stator currents (i^e_{ds}, i^e_{qs}), two rotor fluxes (λ^e_{dr}, λ^e_{qr}) and the mechanical velocity ω_m

$$\begin{aligned}
\dot{x}^e_d &= -cx^e_d + \omega_s x^e_q + n_{\mathrm{p}} b x_4 x_5 + abx_3 + d\left(v^e_d + f^e_d\right)\\
\dot{x}^e_q &= -cx^e_q - \omega_s x^e_d - n_{\mathrm{p}} b x_3 x_5 + abx_4 + d\left(v^e_q + f^e_q\right)\\
\dot{x}_3 &= -ax_3 + aL_{\mathrm{m}} x^e_d + \left(\omega_s - n_{\mathrm{p}} x_5\right) x_4\\
\dot{x}_4 &= -ax_4 + aL_{\mathrm{m}} x^e_q - \left(\omega_s - n_{\mathrm{p}} x_5\right) x_3\\
\dot{x}_5 &= -kfx_5 + m\left(x^e_q x_3 - x^e_d x_4\right) - kT_{\mathrm{L}}
\end{aligned} \tag{1}$$

where the state vector is given by $\left(x^e_d, x^e_q, x_3, x_4, x_5\right)^{\mathrm{T}} = \left(i^e_{ds}, i^e_{qs}, \lambda^e_{dr}, \lambda^e_{qr}, \omega_{\mathrm{m}}\right)^{\mathrm{T}}$. The available and common measurements in a real scenario are given by stator currents $y_d = i^e_{ds}$, $y_q = i^e_{qs}$ and mechanical velocity $y_3 = \omega_m$. Note that, in (1) actuator faults $\left(f^e_d, f^e_q\right)$ are modelled by using an additive structure according to Campos-Delgado and Espinoza-Trejo [15].

3 Fault diagnosis scheme

In this section, the model-based FDI scheme proposed in this paper is detailed. This strategy is derived according to the resulting closed-loop system shown in the Appendix section by following a FOC methodology. Note that two decoupled and linear subsystems are obtained after non-linear feedback. These subsystems are called in this paper as $\Sigma_{f^e_d}$ and $\Sigma_{f^e_q}$, where actuator faults f^e_d and f^e_q originally introduced in (1) still maintain the additive structure in the closed-loop dynamics after the feedback law in (14) (see Appendix)

$$\Sigma_{f^e_d}: \begin{cases} \dot{x}^e_d = -cx^e_d + \left(v^{pi}_d + df^e_d\right)\\ \dot{x}_3 = -ax_3 + aL_{\mathrm{m}} x^e_d\\ y_d = x^e_d \end{cases}$$

$$\Sigma_{f^e_q}: \begin{cases} \dot{x}^e_q = -cx^e_q + \left(v^{pi}_q + df^e_q\right)\\ y_q = x^e_q \end{cases}$$

Also, note that both subsystems $\Sigma_{f^e_d}$ and $\Sigma_{f^e_q}$ are decoupled from operating conditions, and they are only sensitive to a specific fault f^e_d or f^e_q. In this way, by constructing an output observer for each one of these subsystems, a bank of residual generators could be achieved, which will allow to isolate simultaneously the fault set (f^e_d, f^e_q). Nevertheless, note that this neat decoupled structure is based on a feedback law that achieves a decoupling condition in the resulting rotor flux components (see Appendix), and it will not be preserved when an open-circuit fault occurs at the VSI. However, by assuming that the VSI dynamics are much faster than electrical and mechanical time constants of the IM, if the fault vector $\boldsymbol{f}^e_{dq} = \left[f^e_d, f^e_q\right]^{\mathrm{T}}$ can be estimated fast enough and a proper reconfiguration strategy is applied for the VSI, then the closed-loop dynamics in (18) will not be drastically altered, and as a consequence, the mechanical velocity will not be affected. Next in order to obtain a robust model-based FDI scheme, variable structure observers [22] are suggested for this purpose, as described in the following proposition.

Proposition 1: The dynamical structure of the proposed output observer for $\Sigma_{f^e_j}$ subsystem $\forall j \in \{d, q\}$ is conformed by a copy of the subsystem plus linear and non-linear correction terms given by

$$\begin{aligned}
\dot{\hat{x}}^e_j &= -c\hat{x}^e_j + v^{pi}_j + L_j(y_j - \hat{y}_j) + S^j_{\mathrm{obs}}\\
\hat{y}_j &= \hat{x}^e_j
\end{aligned} \tag{2}$$

where $\hat{x}^e_j$ is the estimate of x^e_j, L_j is a constant gain

$$S^j_{\mathrm{obs}} \equiv \begin{cases} \dfrac{K_j\left(y_j - \hat{y}_j\right)}{|y_j - \hat{y}_j|} & \text{if} \quad |y_j - \hat{y}_j| > \varepsilon_j\\ \left(y_j - \hat{y}_j\right) & \text{if} \quad |y_j - \hat{y}_j| \le \varepsilon_j \end{cases}$$

$\varepsilon_j > 0$ is a predefined threshold, and the residual signal is

$$r^e_j = y_j - \hat{y}_j \tag{3}$$

In the absence of the fault $f^e_j = 0$, the error convergence can be guaranteed by selecting the observer gains as

$$\begin{aligned} L_j &> 0\\ K_j &> 0 \end{aligned}$$ □

The proof of this proposition is detailed in the Appendix section. At this point, it is important to remark that the rate of error convergence in both observers can be adjusted by the selection of gains L_j and K_j. Consequently, these values must be chosen to have a much faster response compared with the electrical and mechanical dynamics of the IM. In addition, note that the observer in (2) is of first order $\forall j \in \{d, q\}$. As a result, their real time implementation does not require extra complexity. Finally, note that there is not parameter dependency in the selection of observer gains.

3.1 Fault detection scheme

First, note that when $|y_j - \hat{y}_j| \le \varepsilon_j$ is reached, then, according to (24) in the Appendix, the residual r^e_j dynamical equation is given by

$$\dot{r}^e_j = -\rho\, r^e_j + d\, f^e_j \tag{4}$$

where $\rho = c + L_j + 1$. Thus, the next transfer function is obtained

$$\frac{r^e_j(s)}{f^e_j(s)} = \left(\frac{d}{\rho}\right)\frac{1}{(1/\rho)s + 1} \tag{5}$$

where $r^e_j(s)$ and $f^e_j(s)$ denote the Laplace transforms of the time signals r^e_j and f^e_j. Hence, two new residual signals are proposed, which are defined by r^N_j for $j \in \{d, q\}$ as

$$r^N_j(s) = \left(\frac{\rho}{d}\right) \times r^e_j(s) = \frac{1}{(1/\rho)s + 1} f^e_j(s) \tag{6}$$

where 'N' denotes new residual signals. As a result, the residuals r^N_j $j = \{d, q\}$ achieve a low-pass estimation of the

actuator fault signals f_j^e, where the cut-off frequency in the filters can be adjusted by the observer gains L_j. In this way, fault detection can be carried out by a direct evaluation of the residual vector $\boldsymbol{r}_{dq} = [\Pi]\boldsymbol{r}_{dq}^N$, where $\boldsymbol{r}_{dq} = \left[r_d, r_q\right]^{\mathrm{T}}$ denotes the residual vector in the stator reference frame (dq-coordinates) associated with $\boldsymbol{r}_{dq}^N = \left[r_d^N, r_q^N\right]^{\mathrm{T}}$. Thus, note that $\boldsymbol{r}_{\mathrm{dq}}$ is built starting from residual signal (6) for $j \in \{d,\ q\}$, and applying the following time-varying transformation, which relates dq and dq^N coordinates

$$\Pi \equiv \begin{bmatrix} \cos\theta_s & -\sin\theta_s \\ \sin\theta_s & \cos\theta_s \end{bmatrix} \tag{7}$$

where $\theta_{\mathrm{s}} = \omega_{\mathrm{s}} t$. Hence the residual evaluation can be performed by using a windowed-norm as

$$\|\boldsymbol{r}_{dq}\|_{2,t,T} = \sqrt{\int_{t-T}^{t} \|\boldsymbol{r}_{dq}(t)\|^2 \,\mathrm{d}t} \tag{8}$$

where $\|\cdot\|$ denotes the Euclidean norm. In fact, $\|\boldsymbol{r}_{dq}\|_{2,t,T} \neq 0$ even for a fault free scenario because of measurement noise and model uncertainty. Hence a threshold J_{th} is selected such that

$$J_{\mathrm{th}} = \max_{f_{dq}^e = 0} \|\boldsymbol{r}_{dq}\|_{2,t,T} \tag{9}$$

and a fault is detected if $\|\boldsymbol{r}_{dq}\|_{2,t,T} > J_{th}$. Note that, the window length T has to be selected to balance the tradeoff between robustness and fault sensitivity.

Now, since the residual signals are directly obtained departing from stator currents and their estimates, then, the magnitudes of the residual signals are dependent on the load torque. Therefore in order to correct their scaling for different load torque levels, the residual vector $\boldsymbol{r}_{dq}$ is normalised as shown in (10)

$$r_j^n \equiv \begin{cases} \dfrac{r_j}{\|\boldsymbol{r}_{dq}\|} & \text{if } \|\boldsymbol{r}_{dq}\| > T_h \\ 0 & \text{if } \|\boldsymbol{r}_{dq}\| \leq T_h \end{cases} \tag{10}$$

where T_h denotes a threshold which is used to avoid singularities in this evaluation, 'n' denotes normalised values, $\|\cdot\|$ denotes the Euclidean norm, and the resulting vector is $\boldsymbol{r}_{dq}^n = \left[r_d^n, r_q^n\right]^{\mathrm{T}}$. In this way, the normalised residual signals r_d^n and r_q^n will be used in the isolation stage as describe in the following section.

3.2 Fault isolation scheme

A method to isolate the six faults that can take place in the VSI is suggested in this section. The fault isolation stage is carried out by using the normalised residual vector $\boldsymbol{r}_{dq}^n$, which has been projected from synchronous reference frame into stator reference frame. Note that, this step is necessary because the real actuator faults appear in the abc-frame (see Fig. 1). Furthermore, in the abc-frame, there are six possible faults related to each one of the power switches, but only two residuals are generated $\left(r_d^n, r_q^n\right)$ departing from (r_d^e, r_q^e). Therefore it is argued that residuals (r_d^n, r_q^n) in general have inherited six possible directions, which are associated with each fault, see [15, 23]. Hence, fault isolation could be carried out by analysing the residual phase-portrait after faults. By simplicity the residual vector $\boldsymbol{r}_{dq}^n$ is represented in polar coordinates as

$$\boldsymbol{r}_{dq}^n = \|\boldsymbol{r}_{dq}^n\| \angle \Theta_{dq} \tag{11}$$

In this way, to take a fault isolation decision, it is only necessary to identify the angle Θ_{dq} of the vector $\boldsymbol{r}_{dq}^n$ according to Table 1 by following the previous result in [20]. For a clear perspective, the isolation regions in the dq-plane are illustrated in Fig. 2.

4 Fault compensation strategy

In this section, a fault compensation strategy is suggested by using the information of the model-based FDI stage. This fault compensation strategy has been reported recently in [5], and it is composed of a four-leg inverter in which the fourth inverter leg is used as a hardware redundance (see Fig. 1). Once the faulty leg has been isolated, fault re-configuration is obtained by triggering the appropriate bidirectional switches IS_l and TH_l for all $l = \{a,\ b,\ c\}$. In this way, the motor phase is connected to the back-up fourth-leg for its continuous operation. The most important characteristics about this fault compensation scheme are

- only one faulty-leg can be compensated,
- there is no need for reconfiguration of the control algorithm, and
- two back-to-back thyristors are needed (by leg) to replace the faulty-leg.

5 Experimental evaluation

To validate the ideas presented in this work, an experimental evaluation is carried in a test-bench of 3/4 HP IM. The nominal line voltage and frequency are 230 V rms and 60 Hz, respectively. The IM parameters were identified experimentally according to the algorithm described in [24],

Table 1 Associated angle to each one of the inverter faults

Leg	Switch	Angle
leg-a	S_1, S_4	$240 < \Theta_{\mathrm{dq}} < 300$ or $60 < \Theta_{\mathrm{dq}} < 120$
leg-b	S_3, S_6	$0 < \Theta_{\mathrm{dq}} < 60$ or $180 < \Theta_{\mathrm{dq}} < 240$
leg-c	S_5, S_2	$120 < \Theta_{\mathrm{dq}} < 180$ or $300 < \Theta_{\mathrm{dq}} < 360$

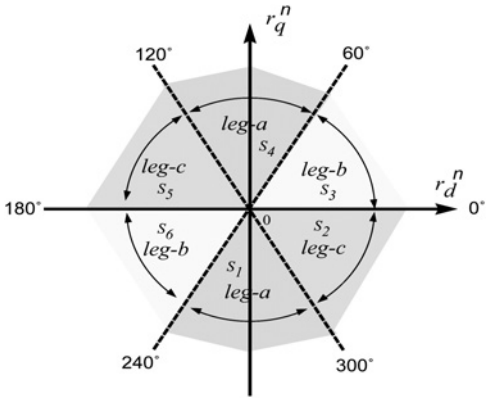

Fig. 2 *Isolation regions in the dq-plane [20]*

doi: 10.1049/iet-pel.2012.0256

and they are listed in Table 2. The PWM inverter is running at a switching frequency of 1 kHz, and the control and diagnostic algorithms are implemented in a DS1103 dSpace board at a sampling frequency of 8 kHz. The switching frequency is limited because of the dSpace 1103 board's characteristics and complexity of the real-time application. It can be considered low for the IM being studied in the laboratory tests. However, for large machines where the implementation of fault tolerant strategies is more important, the switching frequency is not too high for example 2.5 KHz.

For the implemented observers (2), it is only needed two measurements (i_a, i_b) since there is no neutral connection in the stator, that is, $i_c = -(i_a + i_b)$, and the PI control signals (v_d^{pi}, v_q^{pi}) (see Appendix). The gains involved in the FOC algorithm and observers with ($j \in \{d, q\}$) and the fault detection parameters are shown in Table 3. In all experiments, the time window used in (8) was $T = 16$ ms. The power inverter in the test bench (see Fig. 1) is built by using Powerex dual IGBT modules 150 A/1200 V CM150DY-24A with Mitsubishi gate drives M57962 L. The stator currents are measured through LEM transducers LA 55-P. In order to provide a load of the system, a Baldor permanent magnet DC motor 180 V/0.75 HP is coupled to the shaft of the IM that works like a generator. The resulting test bench is illustrated in Fig. 3.

First, an evaluation to load torque variations is carried out in order to show that the residual signals are insensitive to this disturbance. The velocity reference is set to 800 rpm and the flux reference to 0.7 Wb for the FOC system. In this case, it is initially considered 25% of the rated load torque of the IM, and at $t = 2.0$ s there is a step change of 50% rated load torque, see Figs. 4 and 5. Next, it is programmed at $t = 5.0$ s a fault in the upper switch of leg-b (S_3 in Fig. 1). Consequently, the mechanical velocity ω_m presents a small drop because of the input asymmetry, and both residuals r_d^n and r_q^n are activated as illustrated in Fig. 5. Furthermore, the stator currents are distorted after the fault and the estimated rotor flux describes an oscillatory pattern because of the asymmetry in the input voltage (top and middle plots in Fig. 4). The results for the fault detection scheme are showed in Fig. 5. It can be observed in this figure, that fast fault detection could be achieved since it takes only 40.0 ms in order to make a decision. Take into account that

Table 2 Induction motors parameters

Parameter	Value
R_s	8.3861 Ω
R_r	8.3501 Ω
L_s	1.0453 H
L_r	1.0453 H
L_m	0.9589 H
J	0.0084 kgm^2
F	1.3×10^{-3} N.m/(rad/s)

Table 3 FOC algorithm and observer gains

Gain	Value	Gain	Value
k_p^q	10	k_i^q	40
k_p^d	4000	k_p^d	1200
K_j	250	L_j	100
J_{th}	0.4	T_h	2

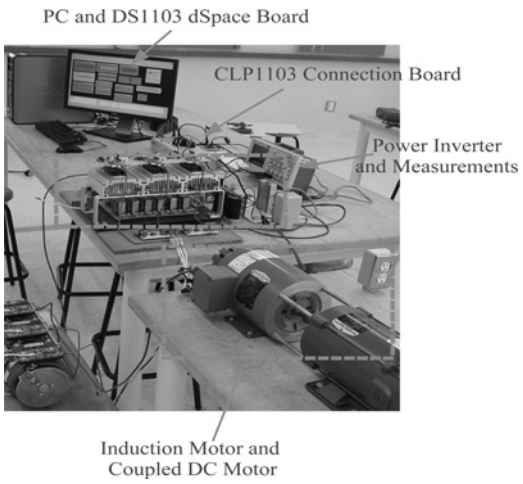

Fig. 3 *Test-bench for experimental validation*

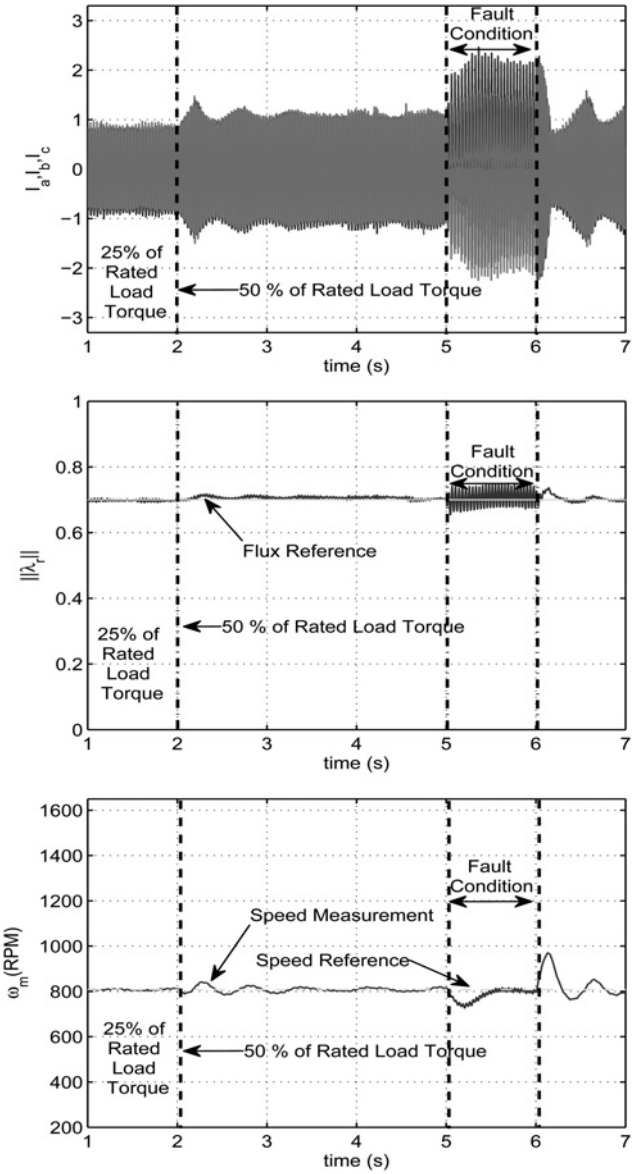

Fig. 4 *Top: stator currents, middle: estimated rotor flux and bottom: mechanical velocity during experimental evaluation of a fault in S_3 switch*

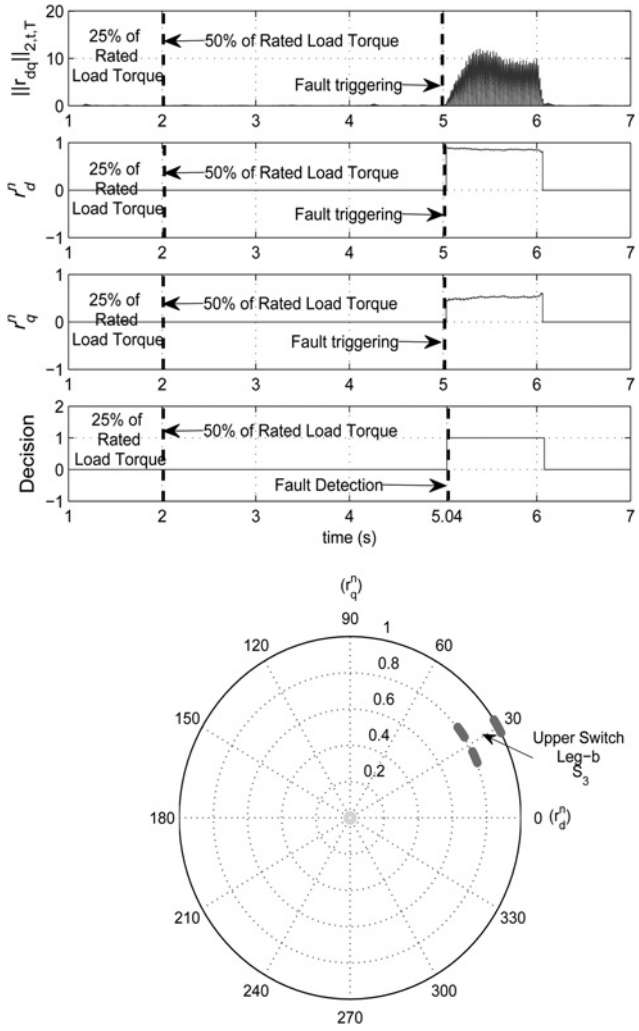

Fig. 5 *Top: detection and residuals signals during experimental evaluation of a fault in S_3 switch, bottom: residual vector in dq-frame $\left(r_d^n, r_q^n\right)$ during experimental evaluation of a fault in S_3 switch*

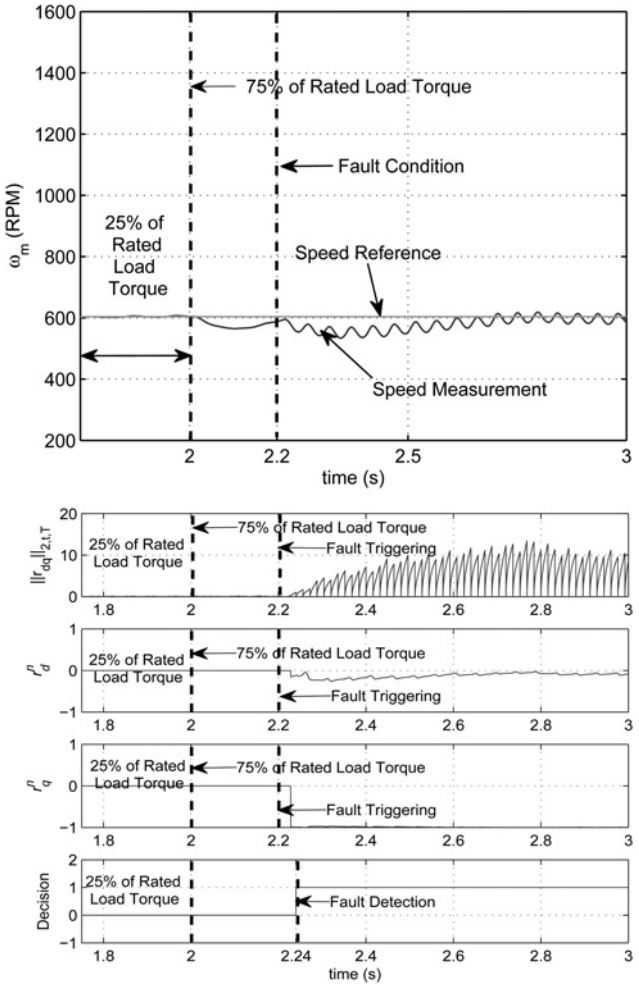

Fig. 6 *Top: mechanical velocity during experimental evaluation of a fault in S_1 switch, bottom: detection and residual signals during experimental evaluation of a fault in S_1 switch*

the fundamental period at this set-point (800 rpm) is 37.5 ms. Now in Fig. 5 (bottom), it is shown the residual vector $\boldsymbol{r}_{dq}^n$ in a phasor representation after fault detection, which is consistent with the description in Table 1 and Fig. 2 for a fault in the upper switch in leg-b of the VSI (S_3). Finally, at $t = 6.0$ s the power inverter is compensated, and the stator currents, estimated rotor flux, and mechanical velocity return to their original steady-state values after some transient time, as shown in Fig. 4. In addition, the automatic FDI scheme does no longer detect a fault in the system (see Fig. 5). Consequently, the proposed scheme is capable of improving the reliability of the closed-loop IM drive, since a fault in the actuator can be effectively detected, isolated and compensated according to the strategy presented in Section 4.

Also, a new experimental evaluation was carried out in order to prove that the proposed FDI scheme is robust under transient operating conditions, as illustrated in Fig. 6. In this case, again it is initially considered 25% of rated load torque for the IM and a set-point frequency of 600 rpm, but next a step change of 75% rated load torque is programmed at $t = 2$ s up to $t = 3.0$ s. After the disturbance, an open-circuit fault is triggered in the upper switch of leg-*a* S_1 at $t = 2.2$ s. It can be observed in Fig. 6 that, the fault condition appears during a transient regime because of the disturbance. Nevertheless, departing from Fig. 6, fault detection scheme is not affected by this unfavourable operating condition. Again, the fault detection task takes only 40 ms in order to make a decision. Take into account that the fundamental period at this set-point (600 rpm) is 50.0 ms.

Fig. 7 illustrates the experimental evaluation of all fault directions for each one of the six switches in the VSI (S_1–S_6) at four different reference velocities (400, 600, 800 and 1000 rpm) and by considering a 30% of rated load torque. In these cases, it is observed separability in the resulting residual trajectories in the *dq*-plane, as expected in Fig. 2. Consequently, by the proposed methodology, each fault could be correctly isolated since the residual is independent of the operating condition. Fig. 7 also shows small angle displacements at the different set-point velocities for the residual trajectories $\left(r_d^n, r_q^n\right)$, which are because of the low-pass filtering property of the residuals in (6).

Finally, two experimental evaluations are carried out in order to test parameter uncertainty in the rotor time constant and observer gains variations. Thus, a deviation of 10 and 25% of the rated rotor resistance parameter was simulated during the experiments. For this, the rated rotor resistance was declared in the algorithm as $R_r^{\text{dev}} = R_r(1 + \Delta)$ with $\Delta = 0.1$ and $\Delta = 0.25$, respectively. Consequently, the real rotor resistance is lower in 10 and 25% to the value used in the

doi: 10.1049/iet-pel.2012.0256

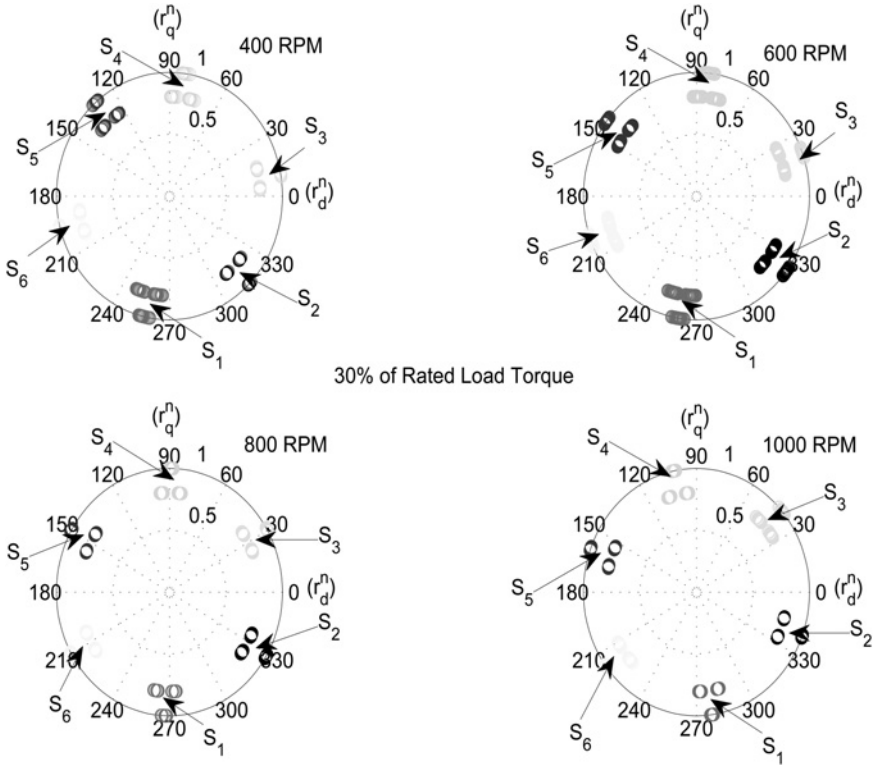

Fig. 7 *Residual vector in dq-frame* $\left(r_d^n, r_q^n\right)$ *during experimental evaluation for all single faults in the VSI at: 400, 600, 800 and 1000 rpm*

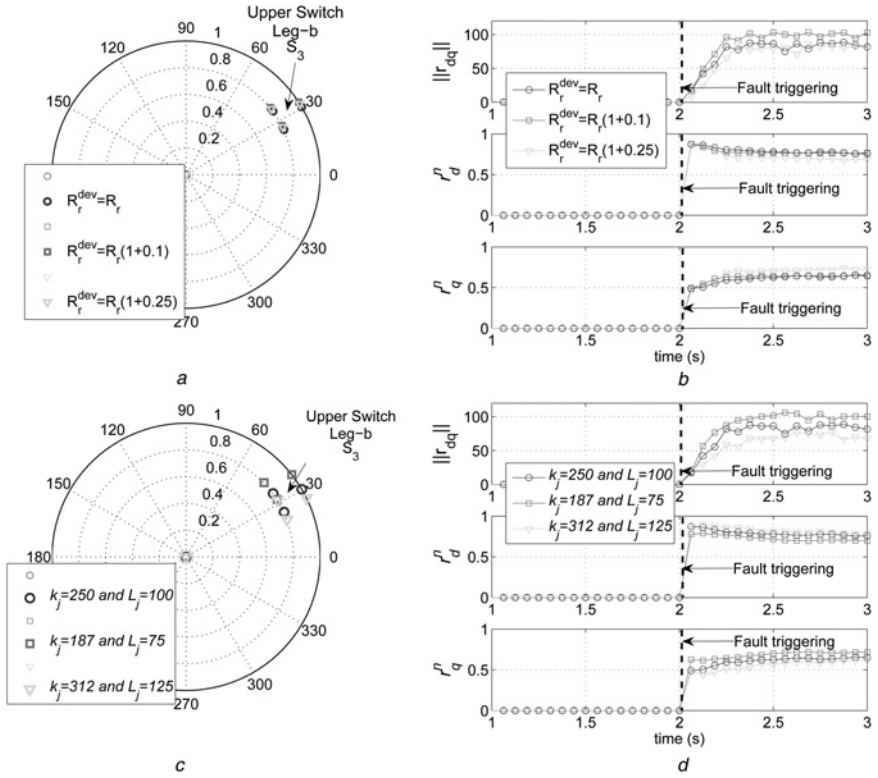

Fig. 8 *Experimental evaluations to test parameter uncertainty in the rotor time constant and observer gains variations*

a Residual vector in *dq*-frame in a phasor representation r_d^n against r_q^n during experimental evaluation for a deviation of 10 and 25% of the nominal value of the rotor resistance

b Magnitude of the residual vector $||\boldsymbol{r}_{dq}||$ and the residual signals $\left(r_d^n, r_q^n\right)$ during experimental evaluation for a deviation of 10 and 25% of the nominal value of the rotor resistance

c Residual vector in *dq*-frame in a phasor representation r_d^n against r_q^n during experimental evaluation for a deviation of $+25$ and -25% of the original values of the observer gains

d Magnitude of the residual vector $||\boldsymbol{r}_{dq}||$ and the residual signals $\left(r_d^n, r_q^n\right)$ during experimental evaluation for a deviation of of $+25$ and -25% of the original values of the observer gains

FDI scheme. Next, a deviation of +25 and –25% of the original observer gains reported in Table 3 was simulated in the experiments. As a consequence, the observer gains were declared as ($K_j = 312$, $L_j = 125$) and ($K_j = 187$, $L_j = 75$), respectively. In both cases, it has been employed a set-point frequency of 600 rpm, and a 50% of the rated load torque. Also, it is programmed at $t = 2.0$s a fault in the upper switch of leg-b (S_3 in Fig. 1). As illustrated in Fig. 8, once more the fault can be properly isolated since the directionality of the residuals in the dq-plane presents robustness to these scenarios.

6 Final remarks

In this paper, it has been showed that decoupled and linear subsystems for FDI purposes can be achieved starting from the closed-loop resulting dynamics by the FOC algorithm. In this case, a bank of variable structure observers was suggested to obtain a robust model-based FDI scheme. In spite of the IM drive running under a closed-loop control action, features of the actuator faults are maintained, so that a qualitative method based on a phasor representation of the residual vector $\boldsymbol{r}_{dq}^{n}$ has been suggested for fault isolation purposes. The proposed FDI scheme was evaluated for single faults and load torque changes at different reference velocities, under transient regimes, and parameter uncertainty on the rotor time constant. Also, it has been demonstrated that fault directionality is preserved for every studied scenario. Finally, it is highlighted that at least one fundamental period of the reference velocity is required for fault detection in our evaluations, as previous approaches in the literature [14]. At this point, the proposed strategy could not be directly extended to address simultaneous faults in the VSI; since in some cases, the induced asymmetry in the stator voltages is so large that the directionality of the residuals is distorted. However, for this purpose, additional information could be incorporated for fault isolation, as estimated rotor fluxes. Therefore as a future work, simultaneous faults in the VSI will be studied in detail. Lastly, note that the necessity of a mechanical sensor is required only in two of the system's stages. The former is associated to rotor flux estimation, which is related to the FOC controller. In this case, the velocity information is considered necessary. On the other hand, the second stage is related to the residual evaluation process, in which the electrical rotor position is employed by the matrix transformation that relates the synchronous reference frame to the stator reference frame. Thus, note that the mechanical sensor's information could be replaced for example by a virtual sensor so that a sensorless application could be adapted for the FDI proposed in this paper.

7 References

1 Fuchs, F.W.: 'Some diagnosis methods for voltage source inverters in variable speed drives with induction machines-a survey'. Proc. IEEE Industrial Electronics. Society Annual Conf., 2003, pp. 1378–1385

2 Yang, S., Bryant, A., Mawby, P., Xiang, D., Ran, L., Tavner, P.: 'An industry-based survey of reliability in power electronic converters', *IEEE Trans. Ind. Appl.*, 2011, **47**, (3), pp. 1441–1451

3 Yang, S., Xiang, D., Bryant, A., Mawby, P., Ran, L., Tavner, P.: 'Condition monitoring for device reliability in power electronic converters: A review', *IEEE Trans. Power Electron.*, 2010, **25**, (11), pp. 2734–2752

4 Smet, V., Forest, F., Huselstein, J.-J., *et al*: 'Ageing and failure modes of IGBT modules in high-temperature power cycling', *IEEE Trans. Ind. Electron.*, 2011, **58**, (10), pp. 4931–4941

5 Zidani, F., Diallo, D., El Hachemi Benbouzid, M., Nait-Said, R.: 'A fuzzy-based approach for the diagnosis of faults modes in a voltage-fed PWM inverter induction motor', *IEEE Trans. Ind. Electron.*, 2008, **55**, (2), pp. 586–593

6 Diallo, D., El Hachemi Benbouzid, M., Hamad, D., Pierre, X.: 'Fault detection and diagnosis in an induction machine drive: a pattern recognition approach based on concordia stator mean current vector', *IEEE Trans. Energy Convers.*, 2005, **20**, (3), pp. 512–519

7 Rothenhagen, K., Fuchs, F.W.: 'Performance of diagnosis methods for IGBT open circuit faults in three phase voltage source inverters for AC variable speed drives'. European Conf. on Power Electronics and Applications, September 2005, pp. 1–10

8 Espinoza-Trejo, D.R., Campos-Delgado, D.U.: 'Detection and isolation of actuator faults for a class of nonlinear systems with application to electric motor drives', *IET Control Theory Appl.*, 2009, **3**, (10), pp. 1317–1329

9 de Araujo Ribeiro, R.L., Jacobina, C.B., da Silva, E.R.C., Lima, A.M.N.: 'Fault detection of open-switch damage in voltage-fed PWM motor drive systems', *IEEE Trans. Power Electron.*, 2003, **18**, (2), pp. 587–593

10 Trabelsi, M., Boussak, M., Mestre, P., Gossa, M.: 'An improved diagnosis technique for IGBTs open circuit fault in PWM-VSI-Fed induction motor drive'. IEEE Int. Symp. on Industrial Electronics, 27–30 June 2011, pp. 2111–2117

11 Lu, B., Sharma, S.K.: 'A literature review of IGBT fault diagnostic and protection methods for power inverters', *IEEE Trans. Ind. Appl.*, 2009, **45**, (5), pp. 1770–1777

12 Abul Masrur, M., Chen, Z., Murphey, Y.: 'Intelligent diagnosis of open and short circuit faults in electric drive inverters for real-time applications', *IET Power Electron.*, 2010, **3**, (2), pp. 279–291

13 Estima, J.O., Marques Cardoso, A.J.: 'A new algorithm for real-time multiple open-circuit fault diagnosis in voltage-fed PWM motor drives by the reference current errors', *IEEE Trans. Ind. Electron.* In Press

14 An, Q.-T., Sun, L.-Z., Zhao, K., Sun, L.: 'Switching function model-based fast-diagnostic method of open-switch faults in inverters without sensors', *IEEE Trans. Power Electron.*, 2011, **26**, (1), pp. 119–126

15 Campos-Delgado, D.U., Espinoza-Trejo, D.R.: 'An observer-based diagnosis scheme for single and simultaneous faults open switch faults in induction motor drives', *IEEE Trans. Ind. Electron.*, 2011, **58**, (2), pp. 671–679

16 Sleszynski, W., Nieznanski, J., Cichowski, A.: 'Open-transistor faults diagnostics in voltage source inverter by analyzing the load currents', *IEEE Trans. Ind. Electron.*, 2009, **56**, (11), pp. 4681–4688

17 Errabelli, R.R., Mutschler, P.: 'Fault-tolerant voltage source inverter for permanent magnet drives', *IEEE Trans. Power Electron.*, 2012, **27**, (2), pp. 500–508

18 De Persis, C., Isidori, A.: 'A geometric approach to nonlinear fault detection and isolation', *IEEE Trans. Autom. Control*, 2001, **46**, (6), pp. 853–865

19 Espinoza-Trejo, D.R., Campos-Delgado, D.U.: 'Actuator faults diagnosis for a class of nonlinear systems applied to electric motor drives'. American Control Conf., Washington, USA, 11–13 June 2008

20 Espinoza-Trejo, D.R., Campos-Delgado, D.U., Loredo-Flores, A.: 'A novel fault diagnosis scheme for FOC induction motor drives by using variable structure observers'. IEEE Int. Symp. on Industrial Electronics, July 2010

21 Krishnan, R.: 'Electric motor drives: Modeling, analysis, and control' (Prentice Hall, 2001)

22 Spurgeon, S.K.: 'Sliding mode observers: a survey', *Int. J. Syst. Sci.*, 2008, **39**, (8), pp. 751–764

23 Espinoza-Trejo, D.R., Campos-Delgado, D.U., Bárcenas, E., Martínez-López, F.J.: 'Robust fault diagnosis scheme for open-circuit faults in voltage source inverters feeding induction motors by using non-linear proportional-integral observers', *IET Power Electron.*, 2012, **5**, (7), pp. 1204–1216

24 Campos-Delgado, D.U., Arce-Santana, E., Espinoza-Trejo, D.R.: 'Edge optimisation for parameter identification of induction motors', *IET Electr. Power Appl.*, 2011, **5**, (8), pp. 668–675

25 Bodson, M., Chiasson, J., Novotnak, R.: 'Nonlinear speed observer for high-performance induction motor control', *IEEE Trans. Ind. Electron.*, 1995, **42**, (4), pp. 337–343

26 Fekih, A.: 'Effective fault tolerant control design for nonlinear systems: application to a class of motor control system', *IET Control Theory Appl.*, 2008, **2**, (9), pp. 762–772

doi: 10.1049/iet-pel.2012.0256

8 Appendix

In this paper, a vector control FOCis employed for the IM drive in order to satisfy high-performance speed control. As a consequence, the FDI stage is formulated by using the resulting closed-loop dynamics obtained after applying the FOC algorithm. This control strategy has been widely studied previously in the literature [25, 26]. The basic principle of this technique consists in holding the magnitude of the rotor flux at a constant value $\lambda^{\star}_{\text{ref}}$. In this way, a linear relationship is obtained between the control variables and velocity. Once the rotor flux has been regulated, then the rotor velocity is asymptotically decoupled from the magnetic flux. Hence, the FOC algorithm has the following three control objectives

$$\lim_{t\to\infty} |\omega_{\text{m}}(t) - \omega^{*}_{\text{m}}| = 0 \tag{12}$$

$$\lim_{t\to\infty} |\lambda^{e}_{dr}(t) - \lambda^{\star}_{\text{ref}}| = 0 \quad \text{and} \quad \lim_{t\to\infty} \lambda^{e}_{qr}(t) = 0 \tag{13}$$

where ω^{*}_{m} denotes the frequency set-point, and $\lambda^{\star}_{\text{ref}}$ the rotor flux reference. These control objectives can be satisfied by using the next control feedback, as showed in [26]

$$\begin{bmatrix} v^{e}_{d} \\ v^{e}_{q} \end{bmatrix} = \frac{1}{d} \begin{bmatrix} -n_p i^{e}_{qs}\omega_m - aL_m \dfrac{i^{e\,2}_{qs}}{\lambda^{e}_{dr}} - ab\lambda^{e}_{dr} + v^{pi}_{d} \\ n_p b\lambda^{e}_{dr}\omega_m + n_p i^{e}_{ds}\omega_m + aL_m \dfrac{i^{e}_{ds} i^{e}_{qs}}{\lambda^{e}_{dr}} + v^{pi}_{q} \end{bmatrix} \tag{14}$$

where the input control v^{pi}_{d} is given by

$$v^{pi}_{d} = k^{d}_{p}\left(\lambda^{\star}_{\text{ref}} - \lambda^{e}_{dr}\right) + k^{d}_{i}\int_{0}^{t}\left(\lambda^{\star}_{\text{ref}} - \lambda^{e}_{dr}(\tau)\right)\text{d}\tau \tag{15}$$

Meanwhile the input control v^{pi}_{q} is expressed as

$$v^{pi}_{q} = k^{q}_{p}\left(\omega^{*}_{m} - \omega_m\right) + k^{q}_{i}\int_{0}^{t}\left(\omega^{*}_{m} - \omega_m(\tau)\right)\text{d}\tau \tag{16}$$

By applying (14), and assuming that

$$\lambda^{e}_{qr} = 0 \quad \text{and} \quad \lambda^{e}_{r} = \lambda^{e}_{dr} \tag{17}$$

the following closed-loop system is obtained

$$\begin{aligned} \dot{x}^{e}_{d} &= -cx^{e}_{d} + \left(v^{pi}_{d} + d\,f^{e}_{d}\right) \\ \dot{x}^{e}_{q} &= -cx^{e}_{q} + \left(v^{pi}_{q} + d\,f^{e}_{q}\right) \\ \dot{x}_3 &= -ax_3 + aL_m x^{e}_{d} \\ \dot{x}_5 &= -kfx_5 + mx^{e}_{q}x_3 - kT_L \end{aligned} \tag{18}$$

Note that the system shown in (18) has a simple dynamic structure: the flux amplitude dynamics are linear and can be independently controlled by v^{pi}_{d}, and the stator currents present a first-order linear description. When the rotor flux x_3 reaches its reference $\lambda^{\star}_{\text{ref}}$, then the dynamics of the speed x_5 are now linear, and can be independently controlled by v^{pi}_{q}. Lastly, gains k^{d}_{p}, k^{d}_{i}, k^{q}_{p}, k^{q}_{i}, must be tuned in order to guarantee stability and tracking performance.

8.1 Rotor flux estimation

The difficulty in direct field oriented control is that the rotor fluxes (λ_{dr}, λ_{qr}) are not directly measurable quantities. However, the rotor flux vector $\lambda_r = [\lambda_{dr}, \lambda_{qr}]^{\text{T}}$ can be estimated departing from the stator phase currents (i_{ds}, i_{qs}), and the mechanical velocity ω_m, as shown in equations (19)–(22)

$$\dot{\lambda}_{dr} = -\frac{R_{\text{r}}}{L_{\text{r}}}\lambda_{dr} - n_p\omega_m\lambda_{qr} + \frac{R_{\text{r}}}{L_{\text{r}}}L_m i_{ds} \tag{19}$$

$$\dot{\lambda}_{qr} = -\frac{R_r}{L_r}\lambda_{qr} + n_p\omega_m\lambda_{dr} + \frac{R_r}{L_r}L_m i_{qs} \tag{20}$$

$$\|\boldsymbol{\lambda}_r\| = \sqrt{\lambda^{2}_{dr} + \lambda^{2}_{qr}} \tag{21}$$

$$\theta_s = \arctan\left(\frac{\lambda_{qr}}{\lambda_{dr}}\right) \tag{22}$$

8.2 Proof of proposition 1

Select a simple Lyapunov function given by

$$V_j(e_j) = \frac{1}{2}e^{2}_{j} \quad j \in \{d, q\} \tag{23}$$

where $e_j = x^{e}_{j} - \hat{x}^{e}_{j}$ denotes the estimation error. Then,

$$\dot{e}_j = -(c + L_j)e_j - S^{j}_{\text{obs}}(e_j) + d\,f^{e}_{j} \tag{24}$$

As a result, by a direct substitution, if the observer gains are selected such that

$$L_j > 0, \;\; K_j > 0 \tag{25}$$

then, when $f^{e}_{j} = 0$ it is satisfied the asymptotic convergence condition

$$\dot{V}_j = -(c + L_j)e^{2}_{j} - K_j e_j S^{j}_{\text{obs}}(e_j) < 0 \tag{26}$$

since the non-linear correction function $S^{j}_{\text{obs}}(e_j)$ fulfills the following conditions,

$$S^{j}_{\text{obs}}(0) = 0,\; e_j S^{j}_{\text{obs}}(e_j) > 0,\; \forall e_j \neq 0,\; e_j \in (-\infty, \infty) \tag{27}$$

□